Chemistry–A European Journal
Research Article
doi.org/10.1002/chem.202302243
Chemistry Europe
European Chemical Societies Publishing
www.chemeurj.org

Special Collection

Ring Strain Energy of Diheteropnictogeniranes El_2Pn (Pn = N, P, As, Sb)– Accurate versus Additive Approaches

Arturo Espinosa Ferao*[a] and Alicia Rey Planells[a]

Dedicated to Professors Alberto Tárraga and Rainer Streubel on their 70th and 65th birthday, respectively.

Accurate ring strain energy (RSE) values for sixty-six parent pnictogeniranes having two other identical p-block elements, El_2Pn, have been reported. A decrease in RSE was observed to correlate with an increase in the p character of the AO used in endocyclic bonds, which is particularly remarkable on descending the groups 15 and 16. The latter also parallels higher -NICS(1) values, which seems not to be related with an increase in aromaticity, as pointed out by other NICS-related criteria, but to atom-centred diatropic currents mostly arising from the presence of lone pairs. Only in case of pnictogenaditrieliranes Tr_2Pn (Tr = B, Al, Ga), the decrease of -NICS(1) is related to a lower Hückel-type 2π-electron aromaticity on descending group 13. The use of an additive methodology based on atom-strain contributions enables estimation of RSEs for a large majority of all possible three-membered rings containing group 13–16 elements with modest accuracy (RMSE = 4.371 kcal/mol), that could be remarkably improved by using bond-strain contributions (RMSE = 1.183 kcal/mol) instead.

Introduction

Three-membered heterocycles containing p-block elements of the periodic table, from the second to the sixth row, represent an interesting balance between reactivity and stability[1] due to their inherent ring strain energy (RSE). The later was found to affect properties such as the stereochemical inversion barriers of $\sigma^3\lambda^3$-pnictogen ring atoms.[2] But, most importantly, the RSE provides the driving force for their transformation into open-chain species, as in the reported enhanced kinetic and thermodynamic reactivity of parent and complexed oxaphosphirane derivatives towards nucleophiles.[3] Furthermore, it is worth noting the connection between a high RSE of any general three-membered ring, denoted as *"c*-XYZ" (or just "XYZ") by its three constituent ring atoms, and its potential increased tendency to undergo ring opening polymerization (*ROP*), giving rise to new polymeric materials -$(X\text{-}Y\text{-}Z)_n$- with properties that *a priori* are still difficult to predict.[4]

The close relationship between the nature of cyclic species and their RSE has led to a growing interest in exploring how this property changes depending on the constituent elements. In this regard, RSE data with high reliability and accuracy have been recently reported, for a large set of rings including the most important three-membered families of parent (unsubstituted) saturated[5] (**I**) and unsaturated[6] (**II**) heterocycles, where X is a group 13–16 element ("El") with its typical covalency completed with H-bonds ($X = ElH_n$), together with a comprehensive analysis of the main factors affecting strain (Figure 1). The study was also extended to rings with three (**III**) or two or identical heteroatoms (**IVa**) as well as the heavier tetreliranes (**IVb,c**,).[7]

In addition, a new fast RSE estimation method, based on the additivity of endocyclic bond contributions $B^{El\text{–}El'}$, was proposed, thus providing an attractive and efficient alternative approach (called RSE^{add}) to the higher-quality (but more tedious) RSE calculation by evaluating homodesmotic reactions.[7] This method can currently be applied to any saturated three-membered ring (3MR) containing only El–El and El–Tt bonds (Tt = C, Si, Ge).

Compared to the above-mentioned rings with tetrel-containing bonds, a significant gap in the literature exists concerning the systematic calculation of RSE for 3MRs having pnictogen atoms. The RSEs for triaziridines[8] and their heavier congeners triphosphiranes[8,9] and triarsiranes[10] were described starting in the late 70ties. Soon later, also the RSE for parent heterocycles El_2Pn (El = C, Si; Pn = N, P)[11] were reported and, more recently, those for CPEl (El = N,[12] O[13] and S[14]) and of inorganic pnictogenditetreliranes Si_2P[15] and Ge_2As.[16]

On the other hand, the potential energy surface of dioxaziridines NO_2[17] as well as the first evidence of their

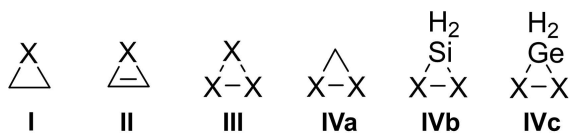

Figure 1. Three-membered heterocycles previously studied.

[a] Prof. Dr. A. Espinosa Ferao, Dr. A. Rey Planells
Department of Organic Chemistry
University of Murcia
Faculty of Chemistry, Campus de Espinardo, E-30100 Murcia (Spain)
E-mail: artuesp@um.es

Supporting information for this article is available on the WWW under https://doi.org/10.1002/chem.202302243

Special Collection Part of a Special Collection on the p-block elements.

experimental existence[18] received early attention and numerous studies on their reactivity as high energy density materials (HEDM) have since then been carried out.[19] However, although the key role of ring strain in HEDM was mentioned, it was not quantified for that ring. Transiently stable zwitterionic Si_2N intermediates and stable Si_2O products were also very recently reported.[20]

In case of tripnictogeniranes, only the RSE for the all *cis* trimethyl-substituted derivative of azadiphosphiridine κ*P*-pentacarbonyltungsten(0) complex (20.98 kcal/mol) was recently reported.[21]

Herein, reference RSE data for parent PnX_2 rings **1**–**4**^{El} ($PnEl_2$ for short, if only the heavy atoms forming the rings are used for naming) (Figure 2) are reported, as well as an analysis of the factors affecting them. In addition, the previously reported additive estimation method for RSE is further refined by employing a wider set of rings and extended to the use of Pn–El bond strain contributions (B^{Pn-El}) that were unavailable beforehand.

Results and Discussion

Accurate RSEs. Scope and limitations

Homodesmotic reactions offer a powerful framework for precisely assessing thermochemical properties in both saturated[5,7] and unsaturated[6] cyclic 3-, 4-, 5-, or 6-membered rings, such as the accurate quantification of ring strain, stability, and reactivity trends, by systematically altering the ring size or formal conversion into acyclic derivatives while maintaining structural integrity. For instance, the significance of homodesmotic reactions in elucidating the intricate interplay of ring size and thermochemical properties was underscored, providing valuable insights for chemical design and prediction.[22] RSEs of all 3MRs herein investigated were calculated using suitable homodesmotic reactions (reaction class 4, or "RC4")[23] (Scheme 1), that were shown[5] to be sufficiently accurate compared to the formally highest ranked, hyper-homodesmotic reactions, the later having the disadvantage of being prone to unwanted uncompensated interactions present in longer chains. The RSE was obtained as the average of the opposite of energetics (including zero-point energy correction) for the three endocyclic bond-cleavage reactions (two of them being identical in this case), at the DLPNO-CCSD(T)/def2-TZVPP(ecp)//B3LYP–D4/def2-TZVP(ecp) level (see computational details) (Table 1).

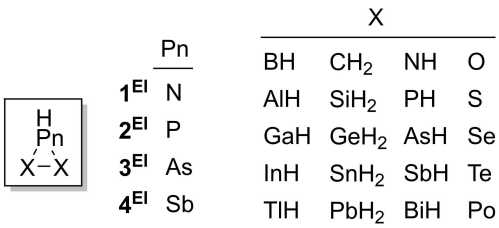

Figure 2. Saturated three-membered heterocycles **1**–**4**^{El} studied.

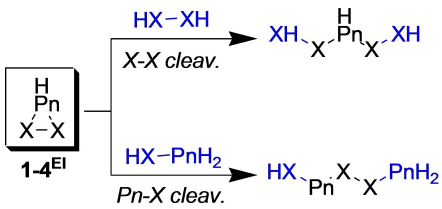

Scheme 1. Homodesmotic (RC4) ring-opening reactions used for the estimation of RSE.

Certain ions of the heaviest elements in Groups 13–15 with a valence two lower than that of their group (Tl(I)), Sn(II), Pb(II) and Bi(III)), and spherically asymmetric atomic electron densities corresponding to a lone pair (LP) that is chemically inert and stereochemically active, result in distorted structures.[24] The case of **1**^{Pb} is interesting because the 6 s^2 LP can be either stereochemically active or inactive in Pb(II) sites, and this is indeed the different behaviour exhibited by every Pb centre in this ring (Figure 3a). This also causes distorted rings for **3**^{In} (Figure 3b). A similar situation occurs with the stereochemically active LP at Sb in **4**^{B} and **4**^{Ga}; on the contrary the Sb centre does not feature such stereochemically active LP in **4**^{Al}, which displays a genuine undistorted (symmetric) ring. Since this type of distorted endocyclic bond cannot be reproduced in the homodesmotic ring opening products, these distorted rings are excluded from the overall computation of RSEs. Related substituent distortions were found in most rings containing El–El bonds between elements with higher metallic character (In, Tl and Pb) and attributed to the presence of endocyclic El–El dative bonds, as already reported in the case of trithallirane, tristannirane and triplumbirane.[7]

At the optimization level, the obtained RSE values (Table S1) are almost systematically overestimated by an average value of 3.21 kcal/mol relative to those at the working level of theory. Moreover, the homodesmotic ring cleavage reactions are sufficiently well chosen to deliver rather similar values, which result in final average RSE values with a low standard deviation average value (Table S2) at both the final ($\sigma = 0.90$ kcal/mol) and optimisation ($\sigma = 1.02$ kcal/mol) levels.

Factors affecting RSE

As observed for previously reported 3MRs,[5,6] the main mechanism of strain relaxation is the effect of LP hybridization.

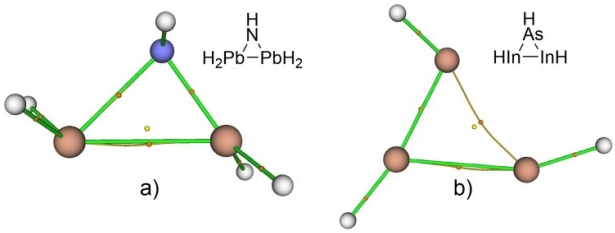

Figure 3. Computed (B3LYP/def2-TZVPP) BCP (small orange spheres), RCP (small yellow sphere), and bond paths for **1**^{Pb} and **3**^{In}.

Table 1. Calculated (DLPNO-CCSD(T)/def2-TZVPP(ecp)) RSE values (kcal/mol) for parent compounds $\mathbf{1}^{El}$, $\mathbf{2}^{El}$, $\mathbf{3}^{El}$, and $\mathbf{4}^{El}$.[a]

$\mathbf{1}^{B}$	36.86	$\mathbf{2}^{B}$	37.39	$\mathbf{3}^{B}$	39.71	$\mathbf{4}^{B}$	–
$\mathbf{1}^{Al}$	37.13	$\mathbf{2}^{Al}$	31.70	$\mathbf{3}^{Al}$	32.10	$\mathbf{4}^{Al}$	32.02
$\mathbf{1}^{Ga}$	40.33	$\mathbf{2}^{Ga}$	36.48	$\mathbf{3}^{Ga}$	37.37	$\mathbf{4}^{Ga}$	–
$\mathbf{1}^{C}$	26.62 (25.9, 26.3,[11a] 27.0,[11b] 28.0, 27.5[11c])	$\mathbf{2}^{C}$	19.73 (24.4, 22.0,[11a] 23.2,[11b] 20.0, 19.4[11c])	$\mathbf{3}^{C}$	18.62	$\mathbf{4}^{C}$	16.67
$\mathbf{1}^{Si}$	38.82 (48.8, 46.1[11a])	$\mathbf{2}^{Si}$	27.70 (32.3 29.9[11a])	$\mathbf{3}^{Si}$	26.97	$\mathbf{4}^{Si}$	25.07
$\mathbf{1}^{Ge}$	41.76	$\mathbf{2}^{Ge}$	29.97	$\mathbf{3}^{Ge}$	29.14	$\mathbf{4}^{Ge}$	27.47
$\mathbf{1}^{Sn}$	39.53	$\mathbf{2}^{Sn}$	29.74	$\mathbf{3}^{Sn}$	28.94	$\mathbf{4}^{Sn}$	27.16
$\mathbf{1}^{N}$	13.96	$\mathbf{2}^{N}$	29.13	$\mathbf{3}^{N}$	23.75	$\mathbf{4}^{N}$	20.83
$\mathbf{1}^{P}$	23.41	$\mathbf{2}^{P}$	6.06	$\mathbf{3}^{P}$	6.05	$\mathbf{4}^{P}$	6.49
$\mathbf{1}^{As}$	18.37	$\mathbf{2}^{As}$	5.98	$\mathbf{3}^{As}$	5.74	$\mathbf{4}^{As}$	6.17
$\mathbf{1}^{Sb}$	19.10	$\mathbf{2}^{Sb}$	7.48	$\mathbf{3}^{Sb}$	7.18	$\mathbf{4}^{Sb}$	5.77
$\mathbf{1}^{Bi}$	16.51	$\mathbf{2}^{Bi}$	6.82	$\mathbf{3}^{Bi}$	6.81	$\mathbf{4}^{Bi}$	6.38
$\mathbf{1}^{O}$	25.50	$\mathbf{2}^{O}$	26.82	$\mathbf{3}^{O}$	26.27	$\mathbf{4}^{O}$	27.70
$\mathbf{1}^{S}$	33.60	$\mathbf{2}^{S}$	16.24	$\mathbf{3}^{S}$	16.65	$\mathbf{4}^{S}$	16.81
$\mathbf{1}^{Se}$	27.95	$\mathbf{2}^{Se}$	15.60	$\mathbf{3}^{Se}$	16.47	$\mathbf{4}^{Se}$	16.20
$\mathbf{1}^{Te}$	29.45	$\mathbf{2}^{Te}$	31.47	$\mathbf{3}^{Te}$	16.37	$\mathbf{4}^{Te}$	16.70
$\mathbf{1}^{Po}$	26.42	$\mathbf{2}^{Po}$	16.39	$\mathbf{3}^{Po}$	15.58	$\mathbf{4}^{Po}$	15.02

[a] Previously reported values in parenthesis.

According to this effect, an increase in the s-character of the LP-containing AO increases the p-character of the AOs used by El in endocyclic bonds, resulting in sp^n-type hybridization with $n > 3$ ("high" p-character, beyond 75%). This approaches the endocyclic bond angles at El to the typical value in related acyclic species thus reducing ring strain.

For the $PnEl_2$ rings under consideration, this LP s-character relaxation effect is observed as a general trend (Figure 4). In general, triels-containing 3MRs are unstable (at least for Tr_3 and $TtTr_2$ rings; Tr = triel; Tt = tetrel),[7] but $PnTr_2$ are comparatively stable, tentatively due to their 2π-electron aromatic character (*vide infra*), although displaying the highest RSEs among pnictogeniranes **1**–**4**, as expected.[5]

Tetrel containing pnictogeniranes (Tt_2Pn) are the next most strained rings, paralleling the tendency observed for mono-heteroatomic saturated 3MRs (C_2El).[5] It is worth noting the significant stabilization of $\mathbf{1}$–$\mathbf{4}^{C}$ with respect to the heavier congeners $\mathbf{1}$–$\mathbf{4}^{Tt}$.

Finally, pnictogeniranes containing (two) additional chalcogen or pnictogen atoms are the least strained rings, as expected. However, a significant increase in the p-character of the AO used by the pnictogen in its endocyclic bonds does not result in the expected relaxation of RSE. As previously observed for symmetric inorganic 3MRs **III**,[7] this destabilizing effect arises from a decrease in the HOMO-LUMO gap, which represents the chemical hardness (η) of a molecule according to Pearson,[25] on descending groups 15 and 16 (Figure 5) except $\mathbf{1}$–$\mathbf{4}^{N}$ and $\mathbf{1}$–$\mathbf{4}^{\circ}$. This in turn arises from a larger increase in HOMO energy (compared to LUMO) (Figures S1 and S2). In case of Tr_2Pn the decrease of the HOMO-LUMO gap is accompanied by a

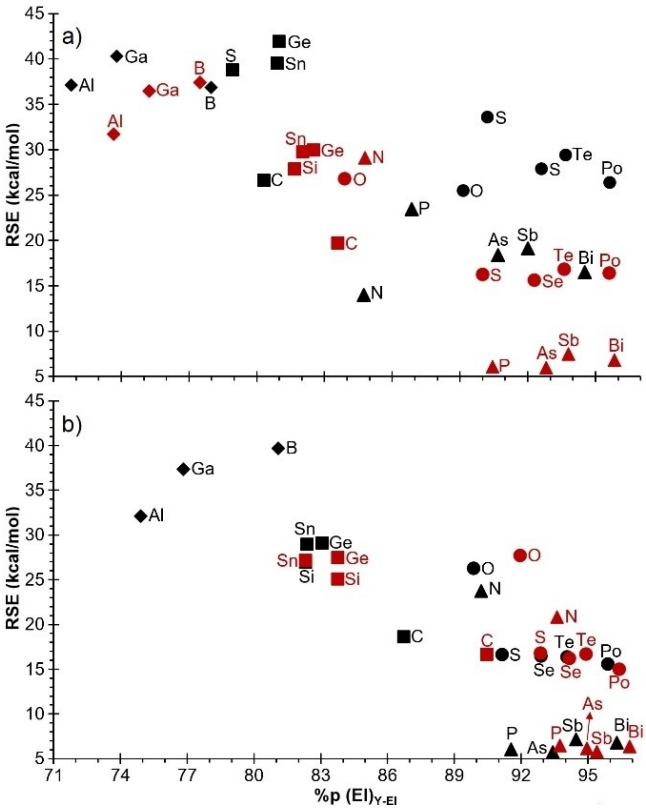

Figure 4. Plots of RSE vs p-character of the AO used by the heteroatom El for its endocyclic Pn–El bonds in $PnEl_2$ rings: a) $\mathbf{1}^{El}$ (Pn: N, black), $\mathbf{2}^{El}$ (Pn: P, red), b) $\mathbf{3}^{El}$ (Pn: As, black), and $\mathbf{4}^{El}$ (Pn: Sb, red). Filled rhombus, squares, triangles and circles for El belonging to groups 13, 14, 15 and 16, respectively.

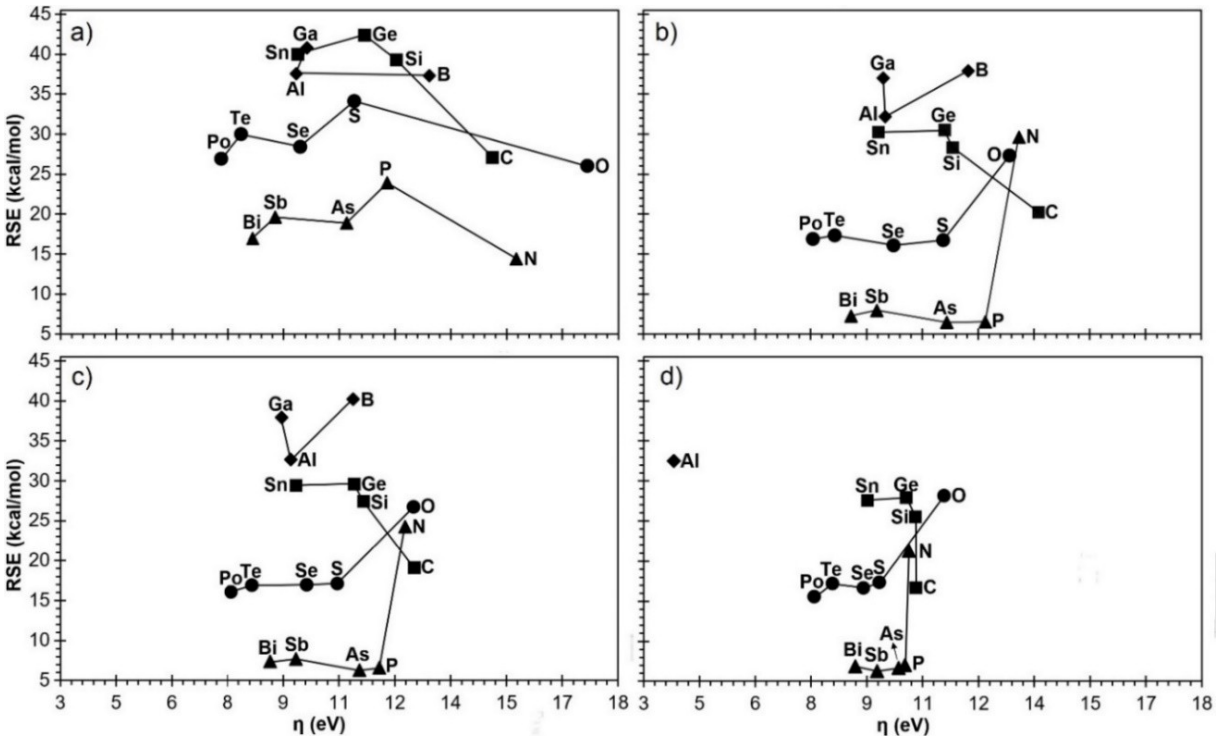

Figure 5. Plots of RSE against chemical hardness (computed as HOMO-LUMO gap) in $PnEl_2$ rings: a) $\mathbf{1}^{El}$ (Pn: N), $\mathbf{2}^{El}$ (Pn: P), b) $\mathbf{3}^{El}$ (Pn: As) and $\mathbf{4}^{El}$ (Pn: Sb). Filled rhombus, squares, triangles and circles for El belonging to groups 13, 14, 15 and 16, respectively.

significant increase of the ring strain, which is damped from the fourth to the fifth row.

It is noteworthy the remarkably high RSE of pnictogenaditrieliranes Tr_2Pn (Tr = B, Al, Ga) with a general decrease in aluminium-containing rings (except for $\mathbf{1}^{Al}$ showing a RSE slightly above $\mathbf{1}^{B}$). Major differences between Al and Ga stem from the fact that, although of an equivalent size ($r_{cov} = 1.25$ Å for both elements), aluminium is more electropositive ($\chi_{Pauling} = 1.61$) than gallium ($\chi_{Pauling} = 1.81$) due to a "d-block" contraction of the electron cloud in the latter. This results in lower Lewis acidity at Tr centres and less hydridic (more covalent) Tr–H bonds in Ga compared to Al. Therefore, aluminium constitutes an inflection point in the lightest triel (B–Al–Ga) series.

Aromaticity studies

Another interesting feature in pnictogenirane El_2Pn rings is the possibility of displaying aromatic character due to the presence of two p electrons in case of triel containing Tr_2Pn rings or six p electrons for Pn'_2Pn or $PnCh_2$ rings. Indeed, all El_2Pn rings exhibit moderate to highly negative NICS(1) (Nucleus Independent Chemical Shift 1 Å above the ring plane) values (Figure 6).

In case of pnictogenaditrieliranes Tr_2Pn (Tr = B, Al, Ga), only boron-containing rings exhibit both a remarkably high -NICS(1) values together with large HOMO-LUMO gaps, thus pointing to a genuine Hückel-type 2π-electron aromaticity (*vide infra*). Moderate -NICS(1) values exhibited by heavier triel derivatives (Al, Ga) may be caused by different phenomena.

On the other hand, potential 6π-electron aromatic rings Pn'_2Pn or $PnCh_2$ display increased -NICS(1) values on descending the respective groups 15 or 16, but paralleling a decrease in the HOMO-LUMO gap. This fact, together with the moderately high -NICS(1) values observed for nonaromatic Tt_2Pn rings (e.g. 10.32 and 11.48 ppm for C_2As and C_2Sb, respectively), could point to diatropic atomic currents, centred at atomic lone pairs, as the source for the resulting high negative values for NICS(1). This phenomenon was previously reported for the non-σ-aromatic Li_3^+ cluster, having two delocalized σ electrons but displaying atom-centred ring currents.[26]

To assess the degree of aromaticity in the rings under consideration, other NICS-based approaches were addressed. With this aim, benzene as well as other clearly aromatic, nonaromatic and antiaromatic 3MRs were also included in this study, for the sake of comparison. Borirene and thiirene rings were included as prototypes of aromatic and antiaromatic three-membered heterocycles, respectively.[6] The reported increase in aromaticity on moving from cyclopropene to the heavier analogue 1*H*-silirene[6] was also explored. Stanger proposed that aromatic rings feature a maximum in their –NICS variation along the perpendicular z axis.[27] The NICS rate variation along the perpendicular z axis and the ratio (NRR) of maximum and minimum in this curve were used as aromaticity criteria.[28] NICS rate is defined as $[NICS(r+\Delta r)-NICS(r)]/\Delta r$. Benzene, borirene, 1*H*-silirene, B_2N and Ga_2N show aromatic-like behaviour as they display one maximum in the plot of –NICS versus distance in the z axis (Figure 7a). Upon inspection of the NICS-rate variation with distance (Figure 7b) a common feature

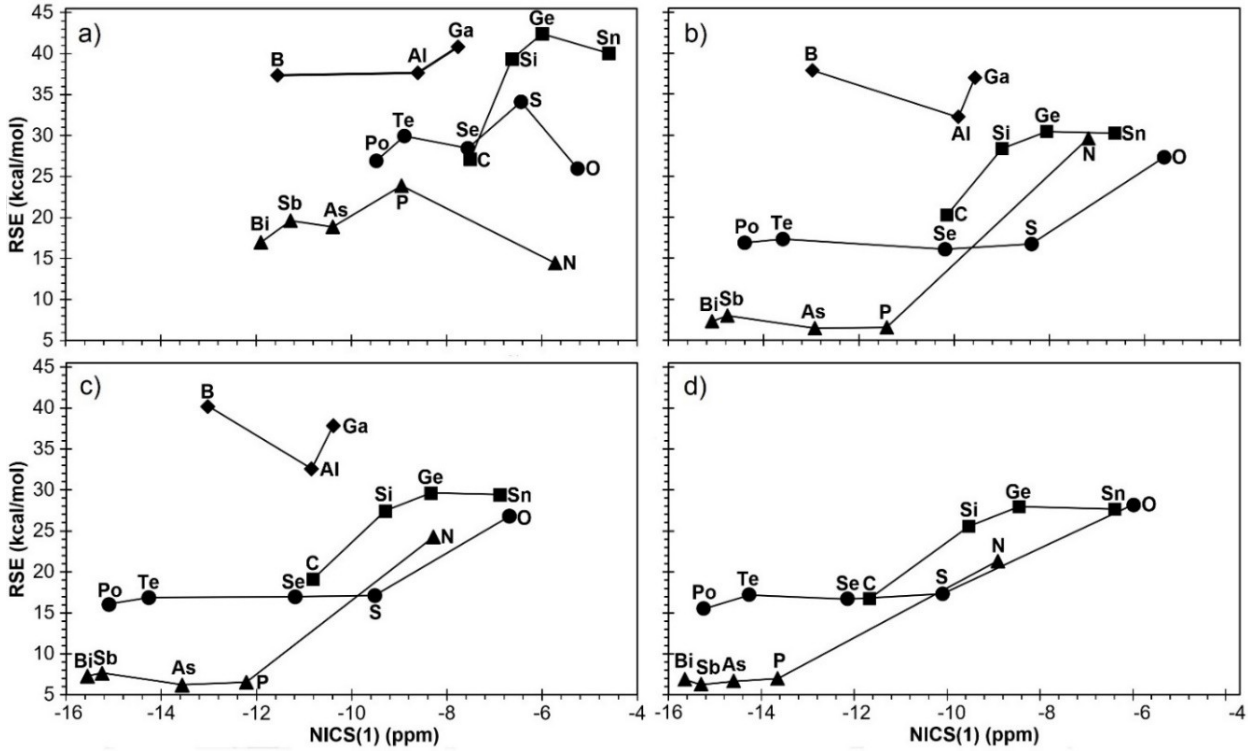

Figure 6. Plots of RSE against NICS(1) in $PnEl_2$ rings: a) $\mathbf{1}^{El}$ (Pn: N), b) $\mathbf{2}^{El}$ (Pn: P), c) $\mathbf{3}^{El}$ (Pn: As) and d) $\mathbf{4}^{El}$ (Pn: Sb).

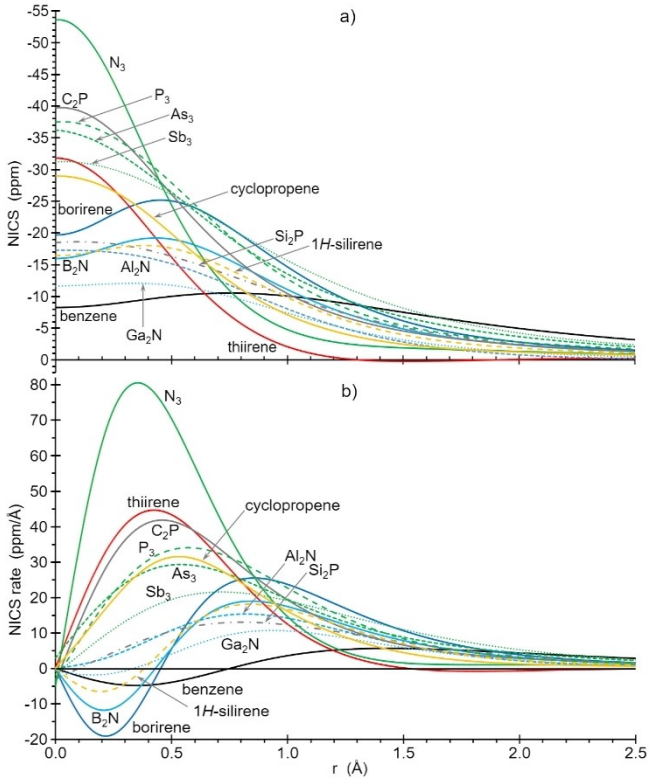

Figure 7. Total NICS (a) and NICS rate (b) variation plots along the perpendicular axis at the ring centroid for selected aromatic, antiaromatic and nonaromatic rings.

is observed for aromatic species: it starts near zero and decreases to a minimum, $(NICS\text{-}rate)_{min}$, then increases across the horizontal axis at the distance corresponding to the maximum of the -NICS function and reaches a maximum, $(NICS\text{-}rate)_{max}$, from which it decreases asymptotically to zero. A modified version of the NICS-rate ratio is herein used (NRR') and defined as the absolute value of the ratio between the minimum and maximum, therefore corresponding to the reciprocal of the previously reported one (NRR).[27] According to the computed NRR' vales the aromaticity in these model ring systems decrease in the order benzene (0.85) > borirene (0.75) > B_2N (0.62) > 1*H*-silirene (0.36) > Ga_2N (0.17).

The only typically antiaromatic thiirene ring exhibits the opposite pattern, starting by an intense maximum and followed by a rather weak minimum, hence having rather small NRR' (0.018). All other studied 3MRs, including Al_2N, C_2P, Si_2P, Pn_3 (Pn = N, P, As, Bi) and cyclopropene, display a unique NICS-rate maximum, with no minimum except at the ring centroid, and can be classified as nonaromatic.

Another NICS-related approach is based on the *free of in-plane component NICS* (FiPC-NICS) reported by Tiznado.[29] The out-of-plane component of NICS ($-{}^1/_3(\sigma_{ZZ})$) is plotted against the in-plane component ($-{}^1/_3(\sigma_{XX}+\sigma_{YY})$) on moving along the perpendicular z axis and starting from the ring centroid (Figure 8).

All four aromatic rings behave in the same way as the curve starts (r = 0.0 Å, at the left-hand side of the curve) by decreasing the out-of-plane NICS component (in case of the 2π electron aromatic rings also the in-plane component negatively in-

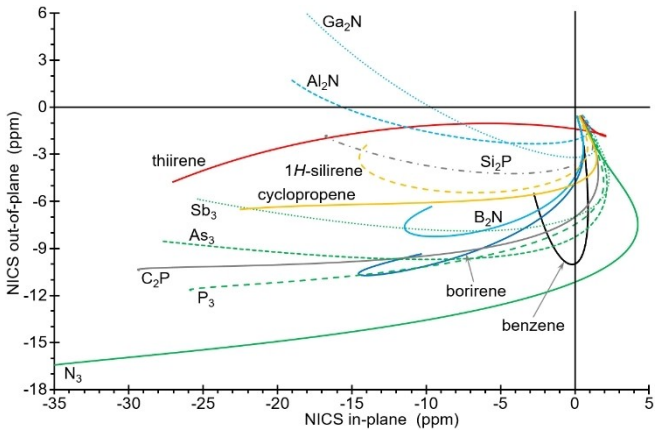

Figure 8. Out-of-plane versus in-plane NICS components variation plot from 0 to 4 Å distance in the z axis perpendicular to the ring plane.

creases at the beginning), reaching a minimum, from which the value increases and vanishes at long distances (herein represented up to 4.0 Å) (Figure 8). The curve starts with negative values for both in-plane and out-of-plane NICS components and crosses the vertical axis (*i.e.* the in-plane component vanishes), the-out-of plane NICS component at this point FiPC-NICS being taken as a measure of aromaticity. FiPC-NICS varies in the order benzene (−9.99 ppm, at r = 1.016 Å) > borirene (−4.83 ppm, at r = 1.642 Å) > B_2N (−4.46 ppm, at r = 1.556 Å) > 1*H*-silirene (−4.06 ppm, at r = 1.486 Å). The curve for the typically antiaromatic thiirene ring starts (r = 0.0 Å) largely dominated by the in-plane component and leads to a rather small FiPC-NICS value (−1.38 ppm, at r = 1.062 Å).

The use of in-plane and out-of-plane representations of NICS components seems not to be able to clearly ascribe the aromatic character of the remaining three-membered rings studied which, in the absence of other diagnostic criteria, could be classified as non-aromatic. An additional criterion was explored for investigating the source of the resulting magnetic shielding observed along the perpendicular z axis. It is based on the pioneering work of Stanger, who plotted NICS–X scans along an axis parallel to the x axis, at z distances ranging from 1.0 to 2.0 Å above the molecular plane,[30] and that of isochemical shielding surfaces (ICSS) of Kleinpeter.[31] The method consists of representing isochemical shielding contour plots (ISCP) in a plane parallel to the ring plane, at 2 Å distance where off-centre effects can be neglected, by using the σ_{zz} component of the magnetic shielding tensor (Figure 9).

In case of the genuinely aromatic borirene ring (a), the highest-value ISCP line covers the whole ring as the magnetic shielding is originated by diatropic ring currents, and the same effect is observed for B_2N (c) and, to some extent, for Ga_2N (e). The ISCP lines are centred at the atom bearing lone pairs in antiaromatic thiirene (b) and also in Al_2N (d) or at the π(C=C) bond in case of cyclopropane (f) and 1*H*-silirene (g). Finally, for the group of tripnictogeniranes, N_3 (h) seems to display a ring centred pattern for the ISCP lines, but they are clearly atom-centred and therefore resulting from atomic diatropic ring currents for the heavier analogues P_3 (i), As_3 (j) and Sb_3 (k).

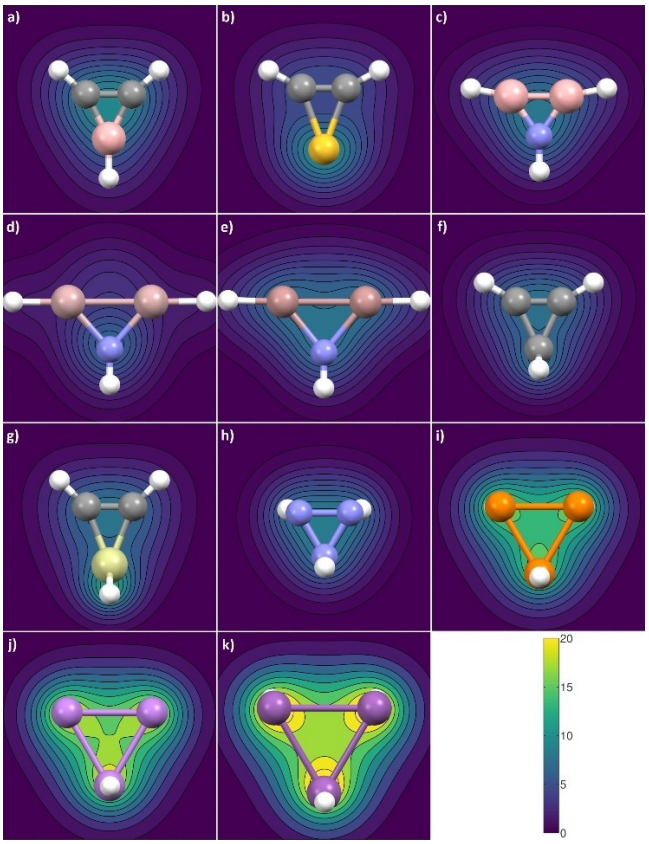

Figure 9. ISCP of σ_{zz} in a plane parallel to the xy (ring) plane and situated ±2 Å away (average) for a) borirene, b) thiirene, c) B_2N, d) Al_2N, e) Ga_2N, f) cyclopropene, g) 1*H*-silirene, h) N_3, i) P_3, j) As_3, k) Sb_3. Contour bar in ppm.

However, the isocontour lines pattern exhibited by N_3 seems to arise also from atomic ring currents displayed at a long distance from the small N atom, as demonstrated by the corresponding plot in a plane 1 Å away from the ring (Figure S3).

Additive Estimation of RSEs

A new rapid methodology for estimating the RSE based on the additivity of the strain contributions of ring constituents (atoms and/or endocyclic bonds) was recently reported,[32] thus providing an attractive and efficient alternative approach to obtain sufficiently reliable RSE values. The chosen method is based on a summation of single bond strain contributions and can currently be applied to any saturated three-membered ring containing only El–El and El–Tt bonds (Tt = C, Si, Ge). The twenty elements contained in the full set of p-block elements in groups 13–16, and from the second to sixth rows, could form up to 1540 different 3MRs, *i.e.* the combinations with repetition of twenty elements taken in groups of three. If the most metallic elements In, Th and Pb are not considered,[5,6] then the possible number of 3MRs with the seventeen remaining elements decreases to 969. The already reported fifty-eight different bond strain contributions *B*, for thirteen El–El and forty-five additional El–Tt (Tt = C, Si, Ge) bonds allowed the

additive estimation of RSE for 388 of these 3MRs, which represents 40.0% of the total amount, with a rather good Root Mean Square Error, RMSE = 1.168 kcal/mol.[32]

The natural extension of this study would be to address $PnEl_2$-type rings (Pn = N, P, As, Sb) in such a way that the method could be expanded to include the contribution of El–Pn bonds to the additively estimated RSE (RSE_B^{add}).

Excluding In, Th and Pb, as mentioned beforehand, and taking into account the previously used rings[32] plus the new fifty-seven rings reported herein, a first approximation would use a set of 136 equations (1) with seventeen unknowns (A_1) corresponding to the number of atoms.

$$RSE_A^{add} = \sum_{i=1}^{3} A_{1i} \quad (1)$$

For instance, a first equation for the $\mathbf{1^B}$ (B_2N) ring would equal its accurate RSE of 36.86 kcal/mol (Table 1) with the summatory $2xA^B + A^N$. For $\mathbf{1^{Al}}$ (Al_2N), the resulting equation is $37.13 = 2xA^{Al} + A^N$, and similarly for the set of 136 rings. Upon numerical resolution of this system and using the previously reported set[32] as initial guess, a new refined set of parameters A_1^{El} (Table 2; "A" stands for atomic and "1" refers to the first approach) with a high RMSE of 4.371 kcal/mol was obtained (mean absolute error, MAE = 3.310 kcal/mol). The resulting values show similar atomic strain contributions for C, N and O, decreasing for heavier chalcogens and, specially, pnictogens (Figure 10). On the contrary heaviest tetrels show enhanced atomic strain contributions, the highest values corresponding to triels.

The rather limited goodness of this first atom-based additive approximation can be visualized when comparing the estimations for the set of 136 rings with the corresponding accurate RSE values obtained through evaluation of homodesmotic reactions (Figure 11a). The plot shows the expected linear correlation although with high dispersion ($R^2 = 0.8402$). Therefore, the first atom-based additive methodology constitutes just a very crude approach for estimating RSEs.

A refinement of the methodology (second approach) consists of using bond-based strain contributions B_2^{El} as

Table 2. Calculated atom- and bond-strain contributions (kcal/mol) A^{El}, B^{El-El}, $B^{El'-El}$ (El': B, Al, Ga, C, Si, Ge, Sn, N, P, As, Sb) to RSE^{add}. In parenthesis the values for the third (atoms&bonds) approximation.

El	A^{El}	B^{El-El}	B^{B-El}	B^{Al-El}	B^{Ga-El}	B^{C-El}	B^{Si-El}	B^{Ge-El}	B^{Sn-El}	B^{N-El}	B^{P-El}	B^{As-El}	B^{Sb-El}
B	16.46 (−5.76)	35.48 (31.72)											
Al	15.38 (0.72)	18.93 (16.55)	28.73 (25.66)										)
Ga	17.36 (0.21)	35.54 (28.29)		27.06 (22.24)									
C	8.65 (−0.69)	8.31 (9.00)	14.97 (18.20)	17.69 (17.68)	17.54 (17.78)								
Si	12.62 (−1.75)	11.62 (13.37)		13.15 (13.67)	14.43 (15.20)	14.28 (15.50)							
Ge	13.13 (0.55)	12.80 (12.25)		13.61 (12.98)	14.92 (14.54)	14.13 (14.20)	12.66 (13.25)						
Sn	12.96 (2.09)	12.11 (10.02)				13.44 (12.74)	11.89 (11.72)	12.28 (10.96)					
N	10.22 (−0.18)	5.34 (5.52)	0.69 (8.42)	9.10 (9.66)	2.39 (5.90)	8.65 (9.09)	15.86 (16.83)	15.38 (15.20)	13.71 (12.76)				
P	3.07 (−2.54)	1.52 (4.05)	0.96 (9.86)	6.38 (8.12)	0.47 (5.16)	6.18 (7.79)	8.58 (10.73)	8.50 (9.49)	8.81 (9.04)	11.42 (12.78)			
As	2.38 (−3.82)	1.66 (5.48)	2.12 (11.66)	6.58 (8.97)	0.91 (6.24)	5.17 (7.43)	7.38 (10.17)	7.93 (9.56)	8.41 (9.28)	8.78 (10.78)	2.21 (5.39)		
Sb	2.02 (−0.20)	2.04 (2.24)		6.54 (7.11)		4.49 (4.94)	6.41 (7.38)	7.00 (6.82)	7.52 (6.58)	8.14 (8.33)	2.60 (3.97)	2.41 (4.42)	
Bi	1.47 (−0.03)	2.31 (2.33)		8.10 (8.58)		2.99 (3.35)	5.05 (5.94)	5.59 (5.33)	6.67 (5.64	7.10 (7.21)	2.26 (3.54)	2.25 (4.18)	2.04 (2.15)
O	10.11 (2.05)	9.14 (7.09)				7.62 (6.94)	12.32 (12.17)	13.19 (11.89)		8.18 (7.24)	8.84 (9.08)	8.56 (9.45)	9.28 (8.35)
S	7.43 (0.23)	9.60 (9.38)				4.83 (5.06)	6.42 (7.18)	7.53 (7.14)		12.00 (11.98)	3.32 (4.47)	3.52 (5.32)	3.60 (3.59)
Se	6.50 (0.44)	8.70 (8.26)				4.50 (4.62)	5.81 (6.47)	6.75 (6.25)		9.62 (9.50)	3.45 (4.50)	3.88 (5.58)	3.75 (3.63)
Te	6.70 (0.45)	9.17 (8.72)				4.19 (4.31)	5.35 (6.00)	6.27 (5.77)		10.14 (10.01)	3.82 (4.87)	3.60 (5.29)	3.77 (3.64)
Po	6.01 (4.56)	8.76 (4.20)				3.50 (1.57)	4.90 (3.49)	5.69 (3.14)		8.83 (6.64)	3.82 (2.81)	3.41 (3.04)	3.13 (0.95)

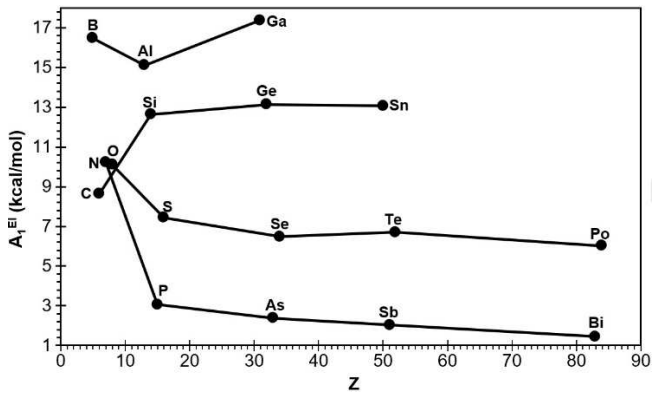

Figure 10. Variation of the calculated atom-strain contributions A_1^{El} (kcal/mol) to RSE_1^{add} with the atomic number.

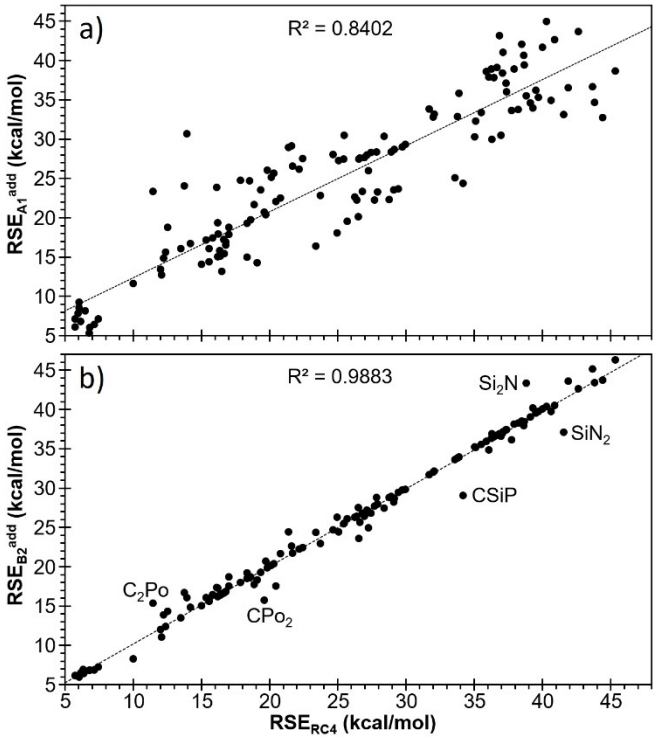

Figure 11. Plot of additively estimated RSE_{A1}^{add} based on atomic contributions (a) and RSE_{B2}^{add} based on bond contributions (b) relative to reference RSE_{RC4}.

addends for the additive estimation of RSE [equation (2)]. By solving the corresponding system of 136 equations with 108 unknowns (50 of which are new), the bond strain contributions are obtained (Table 2) with remarkably lower RMSE of 1.183 kcal/mol (MAE = 0.621 kcal/mol).

$$RSE_B^{add} = \sum_{i=1}^{3} B_{2i} \quad (2)$$

The significant improvement brought by this second approach can be appreciated when comparing the estimated with the accurately computed RSE values for the full set of 136 rings (Figure 11b), displaying a remarkably good linear correlation ($R^2 = 0.9883$). Apart from the significant deviation of the phosphasilirane (CSiP) ring, only the additively estimated RSE for Si–N and C–Po bond-containing rings deviate moderately from the reference values.

This methodology was used to estimate the RSE of a test bed of nine additional rings not included in the set of 136 compounds used to obtain the strain parameters, in order to test its validity and usefulness. The chosen set of rings includes oxaziridines, oxaphosphirane,[3] azaphosphiridine[12a] and the recently reported transient intermediate azasilaalumiridine AlSiN ring.[33] As expected, absolute errors are much lower for bond strain-based additive RSE estimations, except for azaphosphiridine and azasilaalumiridine (Table 3).

Worth is highlighting that the above-mentioned additive methodology based on the enlarged set of 108 bond-strain parameters herein reported, enables the quick and reliable estimation of RSE for 771 rings (80.0% of the maximum number of 969 possible 3MRs that could be formed using the set of seventeen group 13–16 elements from the second to the sixth row, excluding In, Th and Pb).

The third possible approach along this line would consist of making use of both atom- and bond-strain parameters for the additive estimation of RSE. The solution of the over dimensioned system of 136 equations with 125 unknowns (108 bonds and 17 atoms) [equation (3)] led to an insignificant improvement with respect to the previous method (Table 2), with differences in RMSE (1.085 kcal/mol) and MAE (0.621 kcal/mol) below the ninth and seventh decimal place, respectively.

$$RSE_{A\&B}^{add} = \sum_{i=1}^{3} A_{3i} + B_{3i} \quad (3)$$

Therefore, this third, and more complicated, approach does not introduce appreciable quantitative improvements, so that, from a practical point of view, the method of choice for the additive estimation of RSE is the one based on only bond-strain contributions.

Table 3. Calculated (DLPNO-CCSDT/def2TZVPPecp) accurate (RC4) and additively estimated (add) RSEs (kcal/mol) for a testbed of 3MRs.[a]

	RSE^{RC4}	RSE_A^{add}	RSE_B^{add}
Si_2S	24.68	32.67 (7.99)	24.45 (−0.23)
CSiN	39.69	31.50 (−8.19)	38.79 (−0.90)
CSiP	26.79	24.35 (−2.44)	29.04 (2.25)
CSiS	24.40	28.70 (4.30)	25.53 (1.13)
CGeO	37.81	31.89 (−5.92)	34.94 (−2.87)
CPO[b]	22.44	21.84 (−0.60)	22.64 (0.20)
CNO	26.40	28.99 (2.59)	24.45 (−1.95)
CNP[c]	23.70	21.95 (−1.75)	26.25 (2.55)
AlSiN	40.01	39.31 (−0.70)	38.11 (−1.90)

[a] Signed absolute errors in parenthesis. [b] Reported 22.44 kcal/mol.[3] [c] Reported 23.7 kcal/mol.[32]

Conclusions

For sixty-six parent pnictogeniranes rings having two other identical p-block elements, El_2Pn, accurate ring strain energy (RSE) values were computed using homodesmotic reactions and state-of-the-art computational methods. The main electronic factor affecting RSEs was found to be the p character of the AO used in endocyclic bonds, especially for group 15 and 16 elements. The observed increase in magnitude of the rather negative NICS(1) values on descending the groups 15 and 16, cannot be attributed to an increase in aromaticity, but is apparently related to atom-centred diatropic ring currents associated with pnictogen and/or chalcogen lone pairs. On the contrary, the decrease of -NICS(1) values on descending group 13 seems to indicate a decrease of the Hückel-type 2π-electron aromaticity of pnictogenaditrieliranes Tr_2Pn (Tr = B, Al, Ga), as pointed out by the aromatic isotropic ring currents unveiled by the isochemical shielding contour plots at 2 Å distance from the ring plane.

The additive methodology based on the enlarged set of bond strain parameters herein reported, enables the quick estimation of RSE for 771 rings (80.0% of the maximum number of 3MRs that could be formed from seventeen group 13–16 elements from the second to the sixth row), with a remarkably low RMSE = 1.085 kcal/mol (MAE = 0.62 kcal/mol). This acceptable accuracy can only be imperceptibly improved (beyond the ninth and seventh decimal place in RMSE and MAE, respectively) by using a atoms-and-bonds combined methodology. Related additive methodologies could be envisaged for other larger cyclic systems, particularly the similarly strained four-membered rings.

Experimental Section

Density functional theory (DFT) calculations were performed with the ORCA program.[34] All geometry optimizations were run in redundant internal coordinates in the gas phase, with tight convergence criteria, and using the B3LYP[35] functional together with Ahlrichs segmented def2-TZVP basis set[36] and the latest Grimme's semiempirical atom-pairwise London dispersion correction (DFT–D4).[37] From these geometries, all electronic data were obtained through single-point calculations (SP) using the same quality basis set but including additional polarization, def2-TZVPP.[38] Energy values were corrected for the zero-point vibrational term at the optimization level and obtained by the newly developed DLPNO method[39] for the "coupled-cluster" level with single, double, and triple perturbatively introduced excitations (CCSD(T)).[40] Analysis of the hybridization in the AO used for the endocyclic bonds was performed with the NBO method.[41] Properties derived from the topological analysis of the electronic density were obtained with the Multiwfn program.[42] Grid points for calculation of NICS-related properties, isochemical shielding contour plots and the mathematical solution of the systems of equations for the additive methodology were done with GNU Octave scripts.[43] NICS variation plots along the axis orthogonal to the ring plane (z) where computed from 0 to 5 Å, in $\Delta r = 0.002$ Å intervals, starting at the ring centroid. Isochemical shielding contour plots were computed in a plane parallel to the ring (xy) plane, at 2 Å distance, taking points from −3.06 to +3.06 Å in 0.06 Å intervals in both x and y directions (a grid of 10609 equispaced points).

Acknowledgements

The technical support and the computational resources used at the *Servicio de Cálculo Científico* (SCC – University of Murcia) computation center are deeply acknowledged.

Conflict of Interests

The authors declare no conflict of interest.

Data Availability Statement

The data that support the findings of this study are available in the supplementary material of this article.

Keywords: aromaticity · DFT calculation · pnictogen · ring strain energy · three-membered rings

[1] a) P. Kubisa, *J. Polym. Sci. Part A Polym. Chem* **2003**, *41*, 457–468; b) I. C. Stewart, C. Lee, R. G. Bergman, F. D. Toste, *J. Am. Chem. Soc.* **2005**, *127*, 17616–17617.
[2] A. Espinosa Ferao, A. García Alcaraz, *New J. Chem.* **2020**, *44*, 8763–8770.
[3] A. Espinosa Ferao, A. Rey Planells, R. Streubel, *Eur. J. Inorg. Chem.* **2021**, 348–353.
[4] C.-Y. Huang, A. G. Doyle, *Chem. Rev.* **2014**, *114*, 8153–8198.
[5] A. Rey Planells, A. Espinosa Ferao, *Inorg. Chem.* **2020**, *59*, 11503–11513.
[6] A. Rey Planells, A. Espinosa Ferao, *Inorg. Chem.* **2022**, *61*, 6459–6468.
[7] A. Rey Planells, A. Espinosa Ferao, *Inorg. Chem.* **2022**, *61*, 13846–13857.
[8] a) B. M. Gimarc, M. Zhao, *Coord. Chem. Rev.* **1997**, *158*, 385–412; b) C. Leuenberger, L. Hoesch, A. S. Dreiding, *J. Chem. Soc. Chem. Commun.* **1980**, 1197–1198; c) L. Hoesch, C. Leuenberger, H. Hilpert, S. Dreiding, *Helv. Chim. Acta.* **1982**, *65*, 2682–2696; d) A. Karahodza, K. J. Knaus, D. W. Ball, *J. Mol. Struct.: THEOCHEM* **2005**, *732*, 47–53.
[9] a) M. Baudler, B. Carlsohn, W. Böhm, G. Reuschenbach, *Anorg. Chem. Org. Chem.* **1976**, *31*, 558–564; b) M. Baudler, B. Carlsohn, B. Kloth, D. Koch, *Anorg. Allg. Chem.* **1977**, *432*, 67–78; c) S. Chitnis, R. A. Musgrave, H. A. Sparkes, N. E. Pridmore, V. T. Annibale, I. Manners, *Inorg. Chem.* **2017**, *56*, 4521–4537; d) A. Schumann, F. Reiss, H. Jiao, J. Rabeah, J. E. Siewert, I. Krummenacher, H. Braunschweig, C. Hering-Junghans, *Chem. Sci.* **2019**, *10*, 7859–7867.
[10] a) G. Thiele, G. Zoubek, H. A. Lindner, J. Ellermann, *Angew. Chem. Int. Ed.* **1978**, *17*, 135–136; b) M. Baudler, P. Bachmann, *Angew. Chem. Int. Ed.* **1981**, *20*, 123–124; c) C. Spang, F. T. Edelmann, M. Noltemeyer, H. W. Roesky, *Chem. Ber.* **1989**, *122*, 1247–1254; d) A. Schumann, J. Bresien, M. Fischer, C. Hering-Junghans, *Chem. Commun.* **2021**, *57*, 1014–1017.
[11] a) J. A. Boatz, M. S. Gordon, *J. Phys. Chem. A* **1989**, *93*, 3025–3029; b) R. D. Bach, O. Dmitrenko, *J. Am. Chem. Soc.* **2006**, *128*, 4598–4611; c) K. M. Morgan, K. A. Ellis, J. Lee, A. Fulton, S. L. Wilson, P. S. Dupart, R. Dastoori, *J. Org. Chem.* **2013**, *78*, 4303–4311.
[12] a) A. Espinosa, R. Streubel, *Chem. Eur. J.* **2011**, *17*, 3166–3178; b) A. Espinosa, C. Gómez, R. Streubel, *Inorg. Chem.* **2012**, *51*, 7250–7256; c) J. M. Villalba Franco, G. Schnakenburg, T. Sasamori, A. Espinosa Ferao, R. Streubel, *Chem. Eur. J.* **2015**, *21*, 9650–9655; d) A. Rey Planells, A. Espinosa Ferao, *Inorg. Chem.* **2022**, *61*, 13846–13857.
[13] a) O. Krahe, F. Neese, R. Streubel, *Chem. Eur. J.* **2009**, *15*, 2594–2601; b) C. Albrecht, E. Schneider, M. Engeser, G. Schnakenburg, A. Espinosa, R. Streubel, *Dalton Trans.* **2013**, *42*, 8897–8906.
[14] R. Streubel, J. FaBbender, G. Schnakenburg, A. Espinosa Ferao, *Organometallics* **2015**, *34*, 3103–3106.

[15] C. L. Allard, P. Gautier, A. L. Gille, G. E. Thomas, T. M. Gilbert, *Organometallics* **2013**, *32*, 2558–2566.
[16] C. L. Allard, S. T. Gill, T. M. Gilbert, *J. Organomet. Chem.* **2013**, *740*, 110–115.
[17] Y. Li, S. Iwata, *Bull. Chem. Soc. Jpn.* **1997**, *70*, 79–88.
[18] T. Harder, P. Wessig, J. Bendig, R. Stosser, *J. Am. Chem. Soc.* **1999**, *121*, 6580–6588.
[19] A. Rahana, P. M. Fasila, A. Anakuthil, A. R. Biju, *J. Mol. Graphics Modell.* **2021**, *105*, 107863.
[20] R. Holzner, A. Porzelt, U. S. Karaca, F. Kiefer, P. Frisch, D. Wendel, M. C. Holthausen, S. Inoue, *Dalton Trans.* **2021**, *50*, 8785–8793.
[21] A. Schmer, A. García Alcaraz, A. W. Kyri, G. Schnakenburg, A. Espinosa Ferao, R. Streubel, *Dalton Trans.* **2022**, *51*, 3275–3279.
[22] D. H. Ess, K. N. Houk, *J. Org. Chem.* **2007**, *72*, 8310–8317.
[23] S. E. Wheeler, K. N. Houk, P. v. R. Schleyer, W. D. A. Allen, *J. Am. Chem. Soc.* **2009**, *131*, 2547–2560.
[24] A. Walsh, G. W. Watson, *J. Solid State Chem.* **2005**, *178*, 1422–1428.
[25] a) R. G. Pearson, *Coord. Chem. Rev.* **1990**, *100*, 403–425; b) Z. Zhou, R. G. Parr, J. F. Garst, *Tetrahedron Lett.* **1988**, *29*, 4843–4846; c) Z. Zhou, R. G. Parr, *J. Am. Chem. Soc.* **1989**, *111*, 7371–7379; d) R. G. Parr, Z. Zhou, *Acc. Chem. Res.* **1993**, *26*, 256–258; e) G. Makov, *J. Phys. Chem.* **1995**, *99*, 9337–9339; f) Y.-Z. Huang, S.-Y. Yang, X.-Y. Li, *J. Organomet. Chem.* **2004**, *689*, 1050–1056.
[26] A. N. Alexandrova, A. I. Boldyrev, *J. Phys. Chem. A.* **2003**, *107*, 554–560.
[27] A. Stanger, *J. Org. Chem.* **2006**, *71*, 883–893.
[28] S. Noorizadeh, M. Dardab, *Chem. Phys. Lett.* **2010**, *493*, 376–380.
[29] J. J. Torres-Vega, A. Vásquez-Espinal, J. Caballero, M. L. Valenzuela, L. Alvarez-Thon, E. Osorio, W. Tiznado, *Inorg. Chem.* **2014**, *53*, 3579–3585.
[30] R. Gershoni-Poranne, A. Stanger, *Chem. Eur. J.* **2014**, *20*, 5673–5688.
[31] a) S. Klod, E. Kleinpeter, *J. Chem. Soc. Perkin Trans. 2* **2001**, 1893–1898; b) E. Kleinpeter, S. Klod, A. Koch, *J. Mol. Struct.* **2007**, *811*, 45–60.
[32] A. Rey Planells, A. Espinosa Ferao, *Inorg. Chem.* **2022**, *61*, 13846–13857.
[33] M. Ludwig, D. Franz, A. Espinosa Ferao, M. Bolte, F. Hanusch, S. Inoue, *Nat. Chem.* **2023**, DOI: 10.1038/s41557-023-01265-3.
[34] F. Neese, ORCA - An Ab initio, DFT and Semiempirical SCFMO Package, version 4.2.1; Max Planck Institute for Bioinorganic Chemistry, **2019**.
[35] a) C. Lee, W. Yang, R. G. Parr, *Phys. Rev. B* **1988**, *37*, 785–789; b) A. D. Becke, *J. Chem. Phys.* **1993**, *98*, 5648–5652.
[36] F. Weigend, R. Ahlrichs, *Phys. Chem. Chem. Phys.* **2005**, *7*, 3297–3305.
[37] E. Caldeweyher, J.-M. Mewes, S. Ehlert, S. Grimme, *Phys. Chem. Chem. Phys.* **2020**, *22*, 8499–8512.
[38] a) A. Schafer, C. Huber, R. J. Ahlrichs, *Chem. Phys.* **1994**, *100*, 5829–5835. basis sets may be obtained from the Basis Set Exchange (BSE) software and the EMSL Basis Set Library: https://bse.pnl.gov/bse/portal; b) D. Feller, *J. Comput. Chem.* **1996**, *17*, 1571–1586.
[39] C. Riplinger, B. Sandhoefer, A. Hansen, F. Neese, *J. Chem. Phys.* **2013**, *139*, No. 134101.
[40] J. A. Pople, M. Head-Gordon, K. Raghavachari, *J. Chem. Phys.* **1987**, *87*, 5968–5975.
[41] a) A. E. Reed, F. Weinhold, *J. Chem. Phys.* **1983**, *78*, 4066–4073; b) A. E. Reed, R. B. Weinstock, F. Weinhold, *J. Chem. Phys.* **1985**, *83*, 735–746.
[42] T. Lu, F. Chen, *J. Comput. Chem.* **2012**, *33*, 580–592.
[43] J. W. Eaton, D. Bateman, S. Hauberg, R. Wehbring (2023). GNU Octave version 8.2.0 manual: a high-level interactive language for numerical computations. http://www.gnu.org/software/octave/doc/v8.2.0/.

Manuscript received: July 13, 2023
Accepted manuscript online: August 21, 2023
Version of record online: September 28, 2023